Atmospheric Circulation Response to An Instantaneous Doubling of Carbon Dioxide Part I: Model Experiments and Transient Thermal Response in the Troposphere *

Yutian Wu †

Department of Applied Physics and Applied Mathematics, Columbia University, New York, NY

Richard Seager

Mingfang Ting

Naomi Naik

and Tiffany A. Shaw

Lamont-Doherty Earth Observatory, Columbia University, Palisades, NY

Submitted to Journal of Climate on May 24th 2011

*Lamont-Doherty Earth Observatory Contribution Number xxxx.

† *Corresponding author address:* Yutian Wu, Department of Applied Physics and Applied Mathematics, Columbia University, New York, NY, USA

E-mail: yw2225@columbia.edu

ABSTRACT

This study aims to understand the dynamical mechanisms driving the changes in the general circulation of the atmosphere due to increased carbon dioxide (CO_2) by looking into the transient step-by-step adjustment of the circulation. The transient atmospheric adjustment is examined using the National Center for Atmospheric Research Community Atmospheric Model Version 3 coupled to a slab ocean model and the CO_2 concentration in the atmosphere is uniformly and instantaneously doubled. The thermal structure and circulation response is well established after one year of integration with the magnitudes gradually increasing afterwards towards quasi-equilibrium. Tropical upper tropospheric warming occurs in the first month. The expansion of the warming in the middle and upper troposphere to the subtropics occurs later and is found to be primarily dynamically-driven due to the intensification of transient eddy momentum flux convergence and resulting anomalous descending motion in this region. The poleward displacement of the midlatitude tropospheric jet streams occurs together with the change in eddy momentum flux convergence but only after the intensification of the subpolar westerlies in the stratosphere. The results demonstrate the importance of the tropospheric eddies in setting up the extratropical tropospheric response to global warming.

1. Introduction

As the climate warms due to increased greenhouse gases in the atmosphere, the atmospheric general circulation is expected to change. Climate model simulations have found a weakening of the tropical atmospheric circulation (Held and Soden 2006; Vecchi and Soden 2007), a poleward expansion of the Hadley Cell (Lu et al. 2007), a poleward shift of the tropospheric zonal jets (Kushner et al. 2001; Lorenz and DeWeaver 2007) and the midlatitude storm tracks (Yin 2005) as well as a rise in tropopause height (Kushner et al. 2001; Lorenz and DeWeaver 2007). These circulation changes have also been noticed in observational analyses for recent decades (e.g., Hu and Fu 2007; Chen and Held 2007). Stratospheric ozone depletion in the second half of the 20th century might dominate over the role of CO_2 increase in explaining Southern Hemisphere (SH) trends (Polvani et al. 2011; McLandress et al. 2011) and there is a possible contribution from natural variability in both hemispheres (e.g., Seager and Naik 2011).

Some mechanisms have been proposed to understand the cause for the extratropical circulation response to global warming. Lorenz and DeWeaver (2007) suggested that the midlatitude circulation response is predominantly driven by a rise in tropopause height based on the similarities in extratropical circulation response between a simple dry general circulation model (GCM) when the tropopause height is raised and the global warming simulations of models participating in the Coupled Model Intercomparison Project 3 (CMIP3) and assessed by the Intergovernmental Panel on Climate Change Assessment Report Four (IPCC AR4). Lu et al. (2008) proposed two possible mechanisms for the zonal mean circulation response to global warming by analyzing the CMIP3/IPCC AR4 models. The first mechanism suggests that the rising tropospheric static stability stabilizes the subtropical jet streams on the poleward flank of the Hadley Cell, shifting the Hadley Cell, the baroclinic instability zone and the midlatitude eddies poleward. The second mechanism points to the importance of the increased phase speed of the midlatitude eddies. They suggested that the strengthened midlatitude wind in the upper troposphere and lower stratosphere, as a result of enhanced tropical upper tropospheric warming and/or stratospheric cooling along the sloped tropopause, accelerates the eastward phase speeds of the midlatitude eddies, shifting the subtropical breaking region and the transient eddy momentum flux convergence and surface westerlies poleward. Butler et al. (2010) prescribed a heating in the tropical troposphere in a simple atmospheric GCM and found similar poleward jet and storm track displacements as in the CMIP3/IPCC AR4 models, suggesting that the tropical upper troposphere heating drives the circulation response to climate change. Kidston et al. (2010, 2011) found a robust increase in eddy length scale in the CMIP3/IPCC AR4 models, which is possibly caused by increased static stability in the midlatitudes. They argued that the increase in eddy length scale is a possible cause of the poleward shift of the eddy-driven jets and surface westerlies by reducing the eddy phase speed relative to the mean flow on the poleward flank of the jets and shifting the dissipation and eddy source regions poleward.

In addition, the stratosphere and coupling between the stratosphere and the troposphere has also been found to be important in determining the circulation response in the troposphere to global warming. Sigmond et al. (2004) studied the climate effects of middle-atmospheric and tropospheric CO_2 doubling separately using the European Centre Hamburg Model (ECHAM) middle-atmosphere climate model with prescribed sea surface temperatures (SSTs). They found strengthened Northern Hemisphere (NH) midlatitude tropospheric westerlies as a consequence of a uniform CO_2 doubling everywhere in the atmosphere and attributed this mainly to the middle-atmosphere CO_2 doubling.

The mechanisms mentioned above emphasize the close link between the thermal structure and circulation changes to global warming and suggest the warming in the middle and upper troposphere and/or the cooling in the stratosphere as possible causes. The stratospheric cooling is caused directly by increased emission due to increased CO_2 while the middle and upper tropospheric warming in the tropics arises from increased boundary layer temperature and humidity and a shift to a warmer moist adiabatic lapse rate (e.g., Hansen et al. 1984; Held 1993). This explanation for the tropospheric warming is essentially the same as that for the enhanced tropical upper tropospheric warming during El Niños. However, in contrast to the broad warming response under global warming, the heating in the atmosphere during El Niño events is confined in the tropics and anomalous cooling occurs in the midlatitude troposphere induced by anomalous eddy-driven ascending motion (Seager et al. 2003). Also the Hadley Cell strengthens and narrows, and the tropospheric jets and midlatitude transient eddies shift equatorward in response to El Niños. The warming in the middle and upper troposphere in response to global warming, as simulated by the CMIP3/IPCC AR4 models (e.g., Figure 10.7 in Chapter 10 Global Climate Projections for the IPCC AR4), expands beyond the tropical convective region to about 40^oN(S). It is not clear what causes the warming expansion into the extratropics.

In this study, we investigate the transient atmospheric adjustment to an instantaneous doubling of CO_2. The response is investigated using the National Center for Atmospheric Research (NCAR) Community Atmospheric Model (CAM) Version 3 coupled to a slab ocean model. In contrast to previous studies on the equilibrium response to global warming (e.g., Hansen et al. 1984; Manabe et al. 1990; Meehl and Washington 1996; Shindell et al. 2001; Sigmond et al. 2004; Held and Soden 2006; Meehl et al. 2007b; Lu et al. 2008), our work focuses on the transient evolution which allows an assessment of the sequence of cause and effect in the circulation and thermal structure response prior to establishment of a quasi-equilibrium state. Since the actual rate of anthropogenic CO_2 increase is slow compared to the instantaneous CO_2 doubling in our model experiments, the instantaneous CO_2 doubling framework may not be strictly comparable to that in the actual response to global warming in every aspect. However, we demonstrate that our simulations in both transient and equilibrium states agree well with that from the CMIP3/IPCC AR4 models in which the CO_2 concentration is gradually increased. Therefore we believe that the transient atmospheric adjustment to instantaneous CO_2 doubling provides valuable insight into the actual mechanisms underlying the extratropical tropospheric circulation response to global warming. In the paper, the following questions will be addressed: (1) What gives rise to the broad warming in the middle and upper troposphere between 40^{o}S and 40^{o}N? (2) What are the dynamical mechanisms involved in the extratropical circulation response to increased greenhouse gases? First, we describe the model and numerical experiments in Section 2. The quasi-equilibrium response in thermal structure and circulation is presented in Section 3. Furthermore, Section 3 also presents the transient evolution step by step, and in particular, the diagnostics of the cause of the broad warming expansion in the extratropical middle and upper troposphere. Finally, a mechanism of the extratropical tropospheric circulation response to increased CO_2 is proposed. Section 4 extends the analysis of the linkage between the eddy-driven vertical motion anomaly and the warming expansion in the subtropical middle and upper troposphere to 14 CMIP3/IPCC AR4 coupled models. Discussions and conclusions are presented in Section 5. In Part II of the paper, we will mainly focus on the transient, sequential, response day by day before the structure of the extratropical tropospheric circulation response is established, in particular, the perturbations in both the stratosphere and the troposphere and their coupling.

2. Model Experiments

a. Model Description

The NCAR CAM3 is a three-dimensional atmospheric general circulation (AGCM), which includes the Community Land Model (CLM3), an optional slab ocean model, and a thermodynamic sea ice model. There are substantial modifications in the physics and dynamics of CAM3 from the previous version Community Climate Model (CCM3), a detailed description of which is in Collins et al. (2006). CAM3 includes options for Eulerian spectral, semi-Lagrangian, and finite-volume formulations of the dynamical equations. The implementation of CAM3 with T85 spectral dynamics is the version used in the Community Climate System Model Version 3 (CCSM3), which is a fully coupled climate model for the CMIP3/IPCC AR4. CAM3 includes revised parameterizations of cloud condensation and precipitation processes as well as for radiative processes and atmospheric aerosols. The changes to the model lead to a more realistic tropical upper troposphere temperature, a less pronounced double Intertropical Convergence Zone and an improved simulation of tropical continental precipitation. However, biases remain such as the underestimation of the tropical variability associated with the Madden-Julian oscillation, the underestimation of the implied oceanic heat transport in the SH, excessive midlatitude westerlies and surface stress in both hemispheres (Collins et al. 2006; Hurrell et al. 2006; Rasch et al. 2006).

In this study, we use the spectral version of CAM3 with resolution T42L26 (which is equivalent to $2.8^o \times 2.8^o$ (longitude by latitude) horizontal resolution and 26 vertical layers with model top at 2.917mb) coupled to a slab ocean model and a thermodynamic sea ice model (CAM3-SOM). The slab ocean model specifies the observed climatological monthly mean ocean mixed layer depths h and the monthly mean distribution of the ocean heat transport, Q_{flx} ("Q flux"), which is calculated from the surface energy fluxes obtained from a control run with prescribed ice and SSTs (McCaa et al. 2004; Collins et al. 2004). The mixed layer temperature (SST) is the prognostic variable computed from the slab ocean model:

$$\rho_o C_p h \frac{\partial SST}{\partial t} = F_{net} + Q_{flx}, \tag{1}$$

where ρ_o and C_p are density and specific heat capacity of ocean water, respectively, h is the ocean mixed layer depth, F_{net} is the net surface energy flux from the atmosphere to the ocean and Q_{flx} is the prescribed ocean heat transport.

b. Experimental Design

A control experiment of CAM3-SOM is run for 140 years with the CO_2 concentration fixed at 355 ppmv. The year-by-year evolution of the global annual mean surface temperature (T_s) is shown in Figure 1(a) (grey line) and has an average value of 288.5K. The model asymptotes towards an equilibrium state after approximately 40 years (not shown).

Using January 1st of each year of the last 100 years of the control experiment as initial conditions, we generated a 100-member ensemble of single and doubled CO_2 pair runs. The $1CO_2$ run is the same as the control experiment and keeps the CO_2 level constant at 355 ppmv and is integrated forward for 22 years. The double CO_2 experiment is a branch model run lasting for 22 years as well and doubles the CO_2 concentration instantaneously to 710 ppmv at the beginning of the experiment (on January 1st) ($2CO_2$ run). The difference between the $1CO_2$ run and the instantaneous $2CO_2$ run provides the atmospheric response to an instantaneous doubling of CO_2. The ensemble average across the 100 runs to a large extent removes the model's internal variability and allows for an assessment of the day-to-day adjustment of the atmospheric general circulation. Several variables such as zonal and meridional winds, temperature and specific humidity are output daily for the first two years of the model integration. This methodology has been applied successfully to the study of cause and effect in the tropospheric response to El Niño SST anomalies (Seager et al. 2009, 2010a,b; Harnik et al. 2010).

3. Results

a. Global Mean Response

Figure 1 shows the year-by-year evolution of the global annual mean T_s for the $1CO_2$ runs (blue lines) and the $2CO_2$ runs (red lines), for 10 of the 100 ensemble runs. The global annual mean T_s immediately increases by about 0.5 K in the first year after the doubling of CO_2 on January 1st. After about 20 years, the $2CO_2$ runs reach an equilibrium state with T_s asymptoting towards an increase of 2.2 K (shown in Fig. 1(a)(b)).

The CO_2 forcing and the model's climate sensitivity are also examined in the $2CO_2$ runs. Following Gregory et al. (2004), a scatterplot of the ensemble mean change in global annual mean T_s and the change in global annual mean net radiative flux at the top of the atmosphere (TOA) for the 22 years of integration is shown in Figure 2. The intercept of the regression line provides an estimate for the CO_2 forcing at the time of doubling $F_{2\times} = 3.33$ W/m^2 and the slope indicates the climate response parameter $\alpha = 1.54$ W/m^2/K. In Gregory and Webb (2008), they found a doubled CO_2 forcing of 2.93 ± 0.23 W/m^2 and a climate feedback parameter of 1.1 W/m^2/K for the CCSM3 T85 slab ocean model. The two results generally agree with each other despite different horizontal resolutions.

b. Equilibrium Response

As shown in Figure 1, the 2CO_2 simulations reach equilibrium after about 20 years. Figure 3 shows the equilibrium response in zonal mean temperature (T), zonal wind (u), transient eddy momentum flux ($\langle\overline{u'v'}\rangle = \langle\overline{uv}\rangle - \langle\bar{u}\bar{v}\rangle$ [1]) and variance of transient meridional velocity ($\langle\overline{v'v'}\rangle = \langle\overline{vv}\rangle - \langle\bar{v}\bar{v}\rangle$) averaged over 100 ensemble members in year 22 for January-February-March (JFM) and June-July-August (JJA), where bars denote monthly averages and brackets denote zonal averages. The colors show the difference between the 2CO_2 runs and the 1CO_2 runs and the contours show the climatological response from the 1CO_2 runs. The 95% significance level among the 100 ensemble runs is plotted in grey dots. We also estimated the tropopause height as the lowest pressure level at which the temperature lapse rate decreases to 2 K/km following the algorithm in Reichler et al. (2003). Figure 3(a) shows the tropopause level for the 1CO_2 (2CO_2) runs in green (dashed magenta) lines. As expected, the troposphere warms everywhere with a maximum in the tropical upper troposphere, and the stratosphere cools due to additional radiation emission to space. The tropopause height associated with the temperature increase (decrease) in the troposphere (stratosphere) rises by about 5-10mb in the tropics and 10-20mb in the extratropics, which is broadly consistent with Lu et al. (2008). The zonal mean zonal wind response shows a prominent acceleration in the upper troposphere and the stratosphere in both seasons and both hemispheres with the exception of a strong reduction in stratospheric polar jets in JJA in the SH. The zonal wind response in the middle and lower troposphere is less obvious but in the SH there is

[1]Without band-pass filtering.

a clear poleward shift in the tropospheric jet streams and an intensification of about 0.5 m/s on the poleward side of the climatological jets. In the NH, there is a weak poleward shift. These features in equilibrium zonal wind response are also true for the NCAR CCSM3 coupled model simulations (not shown).

The responses in transient eddy momentum flux and variance of meridional velocity include a prominent poleward and upward shift, especially in the upper troposphere and lower stratosphere. There is also an intensification in $\langle\overline{u'v'}\rangle$ on the poleward side of the climatological maxima (NH) and minima (SH), which agrees well with that simulated in the CMIP3/IPCC AR4 coupled models (e.g., Lu et al. 2008; Wu et al. 2010). The change in $\langle\overline{v'v'}\rangle$ is also broadly consistent with that simulated in the CMIP3/IPCC AR4 models (e.g., Yin 2005; Wu et al. 2010; O'Gorman 2010) except the areas of reduction in $\langle\overline{v'v'}\rangle$ on the equatorward flank of the climatological maxima are more pronounced in our experiments. Part of the difference may be due to the lack of a band-pass filter.

The response in transient eddies agrees well with the temperature anomaly and the change in linear baroclinic instability in CAM3-SOM. The largest increase in meridional temperature gradient occurs in the midlatitude upper troposphere and lower stratosphere. This is consistent with the strengthened transient eddies in this region. The close linkage between the thermal structure change and the circulation response to increased greenhouse gases has also been found in other studies (e.g., Yin 2005; Wu et al. 2010; O'Gorman 2010; Butler et al. 2010). Because neither daily variables nor monthly covariances in the NCAR CCSM3 coupled model are available for the CMIP3/IPCC AR4 experiments, the transient eddy activity and its future projections in the coupled model can't be assessed and compared with our results.

c. *Transient Atmospheric Adjustment and Dynamics*

1) Transient Response

Figures 4, 5 and 6 show the month-by-month evolution of $\langle\bar{T}\rangle$, $\langle\bar{u}\rangle$ and $\langle\overline{u'v'}\rangle$ during the first year after the CO_2 concentration is instantaneously doubled on January 1st. The temperature structure and circulation response in the atmosphere are well established during the first year. For example, the pattern correlation between year 1 and year 22 in $\langle\bar{u}\rangle$ is above 0.6 for all months (not shown). The stratospheric cooling in December of year 1 is already similar to that of the equilibrium response (shown in Fig. 3(a)). The tropospheric temperature adjustment also resembles that in equilibrium with a prominent warming in the tropical middle and upper troposphere albeit with lesser magnitude. The stratosphere responds to the CO_2 doubling almost instantaneously and cools by about 2 K in January. The response in the troposphere is slower because of the delay associated with the warming of the oceans followed by transmission of the warming into the troposphere by moist convection and radiation. The middle and upper troposphere in the extratropics only warms up by about 0.5 K in March. The change in tropopause height is quite small in year 1 with the climatological $1CO_2$-run and $2CO_2$-run tropopause heights basically overlaping. The tropopause level, in general, rises by about 2mb except for about 10mb in the NH high latitudes in March of year 1. The westerlies in the stratosphere in both hemispheres intensify strongly and the tropospheric zonal jets shift poleward after March of year 1. This then persists in the SH but weakens due to seasonal variation in the NH. The response in transient eddy momentum flux in the troposphere gets stronger on the poleward side of the climatological jets starting from March of year 1. Similar to the change in tropospheric jets, the strengthening of the transient eddies occurs persistently throughout the year in the SH but has a notable seasonal variation in the NH.

Figure 7(a)(b) show the day-by-day evolution of the zonal mean temperature and zonal wind averaged over 30^oN to 70^oN from January 1st to April 30th of year 1 as a function of time and pressure levels. The average over 30^{o}S to 70^{o}S is shown in Figure 7(c)(d). The response is robust for different choices of latitudinal bands. A 5-day running average has been applied to the variables. The cooling in the stratosphere occurs first in the upper stratosphere and extends to the lower stratosphere in about a month. The substantial warming (0.5 K) in the middle and upper troposphere takes place in early March. The eastward zonal wind anomaly clearly begins in the upper stratosphere and then gradually moves downward into the lower stratosphere and the troposphere with the whole process taking about 100 days. The succession of events, first happening in the stratosphere and subsequently in the troposphere, resembles that in observations of subseasonal to seasonal variability (Baldwin and Dunkerton 2001) as well as in the "downward control" theory (Haynes et al. 1991).

Figure 8 shows the day-by-day response in $\langle \bar{T} \rangle$, $\langle \bar{u} \rangle$, sub-monthly and high-frequency eddy momentum flux convergence as a function of time and latitude in January-February-March-April of year 1. The variables are averaged over the middle and upper troposphere from 150mb to 500mb and a 10-day running average is applied. The eddy momentum flux convergence is defined as $-\frac{1}{acos^2\phi}\frac{\partial(\langle uv\rangle - \langle u\rangle\langle v\rangle)cos^2\phi}{\partial\phi}$, and its high-frequency (transient) component, denoted by $-\frac{1}{acos^2\phi}\frac{\partial\langle u_H v_H\rangle cos^2\phi}{\partial\phi}$, retains the variability with time scales of 2-8 days[2]. As shown in Fig. 8(a), the warming of the middle and upper troposphere first occurs in the tropics and then extends to the subtropics around and beyond 40^{o}N(S) in early March. Almost simultaneously the jet in the middle and upper troposphere is displaced poleward with a reduction in zonal wind equatorward of 40^{o}N(S) and an intensification poleward of 40^{o}N(S) (shown in Fig. 8(b)). The change in eddy momentum flux convergence, and in particular, its high-frequency component, shows a similar transition with a dipole pattern starting from early March of year 1 (shown in Figs. 8(c)(d)). The following section will diagnose the cause of the subtropical warming tendency (diabatic vs. adiabatic) in the middle and upper troposphere focusing on March of year 1.

[2]The time filter used here is a standard 21-point two-sided band-pass filter. It skips the first and last 10 days in the time series of daily eddy momentum flux convergence.

2) CAM3-SOM 2CO2 thermodynamics diagnostics

As mentioned above, the middle and upper troposphere starts to warm up in the subtropics by about 0.5 K in March of year 1. Here we diagnose the primary cause of this expansion of warming by looking into the zonal mean temperature budget following Seager et al. (2003):

$$
\begin{aligned}
\frac{\partial \langle \bar{T} \rangle}{\partial t} = & \underbrace{-\left\{ \frac{\langle \bar{v} \rangle}{a} \frac{\partial \langle \bar{T} \rangle}{\partial \phi} + \langle \bar{\omega} \rangle \left(\frac{\partial \langle \bar{T} \rangle}{\partial p} - \frac{R}{C_p} \frac{\langle \bar{T} \rangle}{p} \right) \right\}}_{\text{(a) MMC}} \\
& \underbrace{- \frac{1}{a cos\phi} \frac{\partial}{\partial \phi} \left\{ \left(\langle \overline{vT} \rangle - \langle \bar{v} \rangle \langle \bar{T} \rangle \right) cos\phi \right\} - \frac{\partial}{\partial p} \left(\langle \overline{\omega T} \rangle - \langle \bar{\omega} \rangle \langle \bar{T} \rangle \right) + \frac{R}{C_p} \frac{1}{p} \left(\langle \overline{\omega T} \rangle - \langle \bar{\omega} \rangle \langle \bar{T} \rangle \right)}_{\text{(b) Eddies}} \\
& \underbrace{+ \frac{\langle \bar{Q} \rangle}{C_p}}_{\text{(c) Diabatic Heating}}, \qquad (2)
\end{aligned}
$$

where the temperature tendency is divided into contributions from (a) the mean meridional circulation (MMC), (b) the transient and stationary eddies and (c) the total diabatic heating Q. The diabatic heating term is the sum of the temperature tendency (T-tendency) due to horizontal diffusion and vertical diffusion, solar heating rate, longwave heating rate, and the heating resulting from shallow, deep-convective, and large-scale condensation processes. Other terms such as the T-tendency due to orographic gravity wave drag and kinetic energy (KE) dissipation are not saved and are neglected in our analysis. However, due to the reformulation of the parameterized heating since CAM2 in order to conserve energy in the model, the KE dissipation term in the surface layer is large ($\approx$ 0.9 K/day) and maximizes in the midlatitude oceanic storm track region where the surface stress is large (Boville and Bretherton 2003). This KE dissipation term results in some discrepancies in the balance in the zonal mean temperature equation in the surface layer (not shown).

Figure 9 shows the latitude-pressure level plot of the net temperature tendency ($\frac{\partial \langle \bar{T} \rangle}{\partial t}$) (Fig. 9(a)), the temperature tendency computed from the RHS of Equation 2 (Fig. 9(b)), the temperature tendencies due to the MMC (Fig. 9(c)), the eddies (Fig. 9(d)) and the total diabatic heating (Fig. 9(f)), separately, during March of year 1. In addition, Figure 9(e) shows the total dynamical contribution, computed as the sum of the MMC and the eddies (Fig. 9(c) and 9(d)). The colors show the difference between the 2CO_2 runs and the 1CO_2 runs and the contours show the results from the 1CO_2 runs. The net temperature tendency (in unit of [K/month]) is estimated as the temperature difference from March 1st to March 31st, which shows a warming tendency in the subtropical middle and upper troposphere from 200mb to 500mb and from 20^{o}N to 45^{o}N (indicated by the black box in Fig. 9) as well as a warming tendency poleward of 50^{o}N. Figure 9(b), in colors, shows the matching temperature tendency computed from the RHS of Equation 2, which, away from the surface, is in good agreement with the actual tendency shown in Fig. 9(a). A comparison between Figs. 9(e) and 9(f) shows that the thermodynamical and dynamical contributions are always opposing each other and it is the dynamical part that leads to the warming tendency in the subtropical middle and upper troposphere. More specifically, the adiabatic warming in the subtropical middle and upper troposphere comes from the anomalous downward vertical motion (Fig. 9(c)) and is opposed by the change in transient eddy heat transport (Fig. 9(d)) and, at lower levels, diabatic heating (Fig. 9(f)). The anomalous downward vertical motion in the subtropical region, in fact, tends to reduce the low-level cloud cover and the condensational heating rate (not shown) and, hence, the total diabatic heating in the region. The polar warming at northern high latitudes is caused by the increased diabatic heating, in particular, the increased longwave radiative heating as a result of increased greenhouse gases (Fig. 9(f)). The temperature tendency diagnosis demonstrates that the warming expansion beyond the tropical convective region is *mainly dynamically driven* and thermodynamically opposed with the circulation change preceding the tropospheric temperature change.

In order to identify the cause for the anomalous vertical motion in the subtropics, we have computed the eddy-driven vertical motion ω_{eddy}. It is derived using the continuity equation and the balance between the Coriolis torque and the momentum flux convergence, which is the dominant balance in the extratropics in the zonal momentum equation, following Seager et al. (2003):

$$\langle \bar{\omega}_{eddy}(p) \rangle \;=\; \langle \bar{\omega}(p_o) \rangle - \frac{1}{acos\phi} \frac{\partial}{\partial \phi} \times \int_{p_o}^{p} \frac{1}{acos\phi} \frac{1}{f + a^{-1}\langle \bar{u} \rangle tan\phi} \frac{\partial}{\partial \phi} \Big(\langle \overline{u'v'} \rangle cos^2\phi \Big)\; dp, \quad (3)$$

where p_o is taken to be 100mb. This is, in fact, the downward motion controlled by the wave forcing above in the "downward control" principle in Haynes et al. (1991) except in the conventional Eulerian framework. The eddy-induced motion ω_{eddy} was computed at all pressure levels using $\langle \bar{u} \rangle$ and $\langle \overline{u'v'} \rangle$ from the model output[3]. Figure 10 shows ω_{eddy} computed from Equation 3 and the actual vertical motion ω from the model output in March of year 1 (Note, the values of ω_{eddy} are large in the surface layer because of neglect of surface friction.). In both hemispheres there is reasonable agreement in the meridional structure of the actual vertical velocity and the eddy-induced vertical velocity away from the tropics in both the climatological 1CO_2 runs (shown in contours) and the 2CO_2-run anomalies (shown in colors). The anomaly in ω_{eddy} is primarily attributed to the change in $\langle \overline{u'v'} \rangle$. As shown in Fig. 10(b), there is an anomalous ascending motion in the NH tropics driven by enhanced tropical convective heating following the CO_2 increase which is consistent with the increased diabatic heating in the region (Fig. 9(f)). In the NH subtropics (between 30^oN and 45^oN), there is a descending motion anomaly which also shows up in the change in ω_{eddy}. This indicates that the anomalous downward motion is primarily driven by the enhanced transient eddy momentum flux convergence. The Hadley Cell expansion as found in CMIP3/IPCC AR4 coupled models (Lu et al. 2007) is also presumably related to the changing transient eddies in this region.

The heating anomaly in the subtropical middle and upper troposphere in this model experiment is induced by the dynamical circulation change rather than vice versa. It is the enhanced transient eddy momentum flux convergence in response to increased CO_2 that causes anomalous descending motion and adiabatic heating in the subtropical middle and upper troposphere. The dynamics of the changing transient eddies is closely connected with

[3] There is a $\cos\phi$ term missing in the denominator of Equation (7) in Seager et al. (2003).

the response in the stratosphere and coupling between the stratosphere and the troposphere, and this will be further investigated in Part II.

d. *Possible Dynamical Mechanisms*

Based on the above diagnostic work, we propose a possible dynamical mechanism for the extratropical circulation response to increased CO_2 with the following sequence:

(1) The CO_2 doubling gives rise to a westerly zonal wind anomaly in the stratosphere.

(2) The westerly acceleration in the lower stratosphere and upper troposphere changes the propagation of baroclinic eddies, leading to enhanced transient eddy momentum flux convergence between 40^oN(S) and 60^oN(S).

(3) The increased transient eddy momentum flux convergence drives an anomalous mean meridional circulation in the troposphere as well as a poleward displacement of the tropospheric jets.

(4) The induced anomalous descending motion in the subtropical middle and upper troposphere leads to an adiabatic heating anomaly and thus a broad warming expansion beyond the tropical convective region. The subtropical warming allows adjustment to thermal wind balance with the poleward shifted jets.

A schematic figure showing the hypothesized sequence of the dynamical response is shown in Figure 11. Other mechanisms are also possible. For example it is expected that the increase in tropopause height could cause an increase in the length scale of transient eddies which has been associated with a poleward jet shift (Williams 2006). The dynamical mechanisms of the transient adjustment and their cause and effect, explaining all possibilities, will be analyzed in detail in Part II.

4. Eddy-Driven Vertical Motion in CMIP3/IPCC AR4 Coupled Models

The work so far has demonstrated the importance of the eddy-driven vertical motion in inducing the warming anomaly in the middle and upper troposphere from our instantaneous CO_2 doubling experiments in CAM3-SOM. This section extends the work to an ensemble of CMIP3/IPCC AR4 coupled models (Meehl et al. 2007a) and shows that the above conclusions also apply in these models. Because the CMIP3/IPCC AR4 SRES A1B experiments are quasi-equilibrium runs and the diabatic heating term is not available in the standard output, we can't examine the causality sequence or close the zonal mean temperature equation as in previous section. Instead we calculate the eddy-driven vertical motion ω_{eddy} from Equation (3) using the transient eddy momentum flux $\langle\overline{u'v'}\rangle$ from model output and compare it to the total vertical motion ω. Table 1 lists the 14 models used in this analysis. These models are chosen based on the availability of daily variables for both the 20C3M runs (1961-2000) and the SRES A1B runs (2081-2100). They are the same models analyzed in Seager et al. (2010c) except for the Institute for Numerical Mathematics Climate Model, Version 3.0 (INMCM3.0) which has no available output for 2081-2100. The late 21st century trend is defined as the difference between 2081-2100 and 1961-2000.

Figure 12 shows the multi-model annual average of $\langle\bar{T}\rangle$, $\langle\bar{u}\rangle$, $\langle\overline{u'v'}\rangle$, $\langle\overline{u_H v_H}\rangle$, $\langle\bar{\omega}_{eddy}\rangle$ and $\langle\bar{\omega}\rangle$ for the 1961-2000 climatology (shown in black contours) and the late 21st century trend (shown in colors) in the troposphere from 200mb[4] to 1000mb. The high-pass filter again retains the variability of time scale 2-8 days. As is expected, there is a broad temperature increase in the whole troposphere. For example, the 4K temperature increase extends to about 40^{o}S and 50^{o}N. Both the tropospheric jets and (high-frequency) transient eddy momentum flux shift poleward with an intensification on the poleward flank. There is also an anomalous downward motion in the subtropics between 30^{o}N(S) and 50^{o}N(S).

[4]Daily atmosphere data are output to standard levels up to 200mb.

The agreement between ω_{eddy} and ω in both the location and amplitude supports the idea that the descending motion anomaly is driven by the enhanced transient eddy momentum flux convergence, primarily via the high-frequency component. This is a robust feature for each of these 14 models except for the IAP FGOALS. Therefore, the linkage between the eddy-driven vertical motion anomaly and the subtropical warming expansion in the middle and upper troposphere is consistent with the CAM3-SOM results although the cause and effect can't be assessed for the CMIP3/IPCC AR4 models.

5. Discussions and Conclusions

We have explored the transient evolution of the atmospheric adjustment to an instantaneous doubling of CO_2 concentration. The sequence in the general circulation response in the atmosphere helps reveal the dynamical mechanisms underlying the equilibrium circulation response, for example, the poleward expansion of the Hadley Cell (Lu et al. 2007), and the poleward shift of the tropospheric jets and storm tracks (e.g., Kushner et al. 2001; Yin 2005) as found in CMIP3/IPCC AR4 models. In contrast to previous studies suggesting that the thermal forcing in the tropical upper troposphere drives the tropospheric circulation response (e.g., Lu et al. 2008; Butler et al. 2010), our results indicate that the broad warming expansion in the subtropical middle and upper troposphere is a consequence of the circulation change. Enhanced transient eddy momentum flux convergence in the lower stratosphere and upper troposphere, possibly originating from the stratospheric westerly acceleration, drives an anomalous mean meridional circulation in the troposphere. The induced anomalous descending motion in the subtropical middle and upper troposphere warms the air adiabatically. Afterwards the subtropical warming and the poleward displacement of the jets and the baroclinic eddies can potentially feed back positively onto each other via a poleward shift in eddy generation region, leading to a further poleward shift of the jets and the eddies and a further warming expansion in the subtropical troposphere.

Our results also show the sequence of the zonal wind anomaly in the vertical column of the atmosphere, indicating that the poleward displacement of the tropospheric jets follows the subpolar westerly anomaly in the stratosphere. It suggests the importance of the stratosphere, and the coupling between the stratosphere and the troposphere, in regulating the extratropical tropospheric circulation response to increasing CO_2. A detailed analysis of the stratospheric response and the stratosphere-troposphere coupling, including how the response 'propagates' downward into the troposphere and how the eddies respond step-by-step will be further examined in Part II. It is noted here that our study intends to understand the circulation response and the dynamical mechanisms in CMIP3/IPCC AR4-like models albeit most of the models have poorly resolved stratospheres. Some studies have argued that a well resolved stratosphere is required to reproduce the observations (e.g., Shindell et al. 1999; Sassi et al. 2010). On the other hand, Sigmond et al. (2008) suggested that the atmospheric circulation response to CO_2 doubling does not necessarily require a well-resolved stratosphere but rather a realistic simulation of the zonal wind strength in the middle and high latitude lower stratosphere. The zonal mean zonal wind in CAM3 agrees with reanalysis data in this region. The circulation response to a CO_2 doubling in both the troposphere and the stratosphere in our results also agrees to a large extent with those from previous studies, which used models with much finer vertical resolution in the middle atmosphere (e.g., Shindell et al. 2001; Sigmond et al. 2004). However, a model lid in the mid-stratosphere is known to impact the vertical propagation of stationary planetary scale waves during northern hemisphere winter (Shaw and Perlwitz 2010; Sassi et al. 2010). Assessing the transient and equilibrium responses to CO_2 doubling in a model with high vertical resolution and a high model lid height is the subject of future investigation. Finally, as our experiments double the CO_2 concentration on January 1st, it would be interesting to change the time of CO_2 doubling and see if the model responds differently. A set of experiments with an instantaneous CO_2 doubling on July 1st is currently under investigation.

Acknowledgments.

YW was supported by NASA Headquarters under the NASA Earth and Space Science Fellowship Program-Grant NNX08AU80H. RS, MT and NN were supported by NOAA awards NA08OAR4320912 and NA10OAR4320137 and NSF awards ATM-0804107. TAS was supported by a postdoctoral fellowship from the Natural Sciences and Engineering Research Council of Canada. The authors would like to thank the Global Decadal Hydroclimate (GloDecH) group at Lamont-Doherty Earth Observatory and Columbia University for their comments and advice, in particular, Prof. Lorenzo Polvani and Dr. Michela Biasutti as well as Dr. Nili Harnik. We also thank helpful discussions with Profs. Ngar-Cheung Lau, Geoffrey K. Vallis and Benjamin Lintner.

REFERENCES

Baldwin, M. P. and T. J. Dunkerton, 2001: Stratospheric harbingers of anomalous weather regimes. *Sci.*, **294 (5542)**, 581–584.

Boville, B. A. and C. S. Bretherton, 2003: Heating and kinetic energy dissipation in the NCAR Community Atmosphere Model. *J. Clim.*, **16**, 3877–3887.

Butler, A. H., D. W. J. Thompson, and R. Heikes, 2010: The steady-state atmospheric circulation response to climate change-like thermal forcings in a simple general circulation model. *J. Clim.*, **23**, 3474–3496.

Chen, G. and I. M. Held, 2007: Phase speed spectra and the recent poleward shift of Southern Hemisphere surface westerlies. *Geophys. Res. Lett.*, **34**, L21 805, doi:10.1029/2007GL031 200.

Collins, W. D., et al., 2004: Description of the NCAR Community Atmosphere Model (CAM3.0). Tech. rep., Climate And Global Dynamics Division, National Center For Atmospheric Research, Boulder, Colorado, USA.

Collins, W. D., et al., 2006: The formulation and atmospheric simulation of the Community Atmosphere Model version 3 (CAM3). *J. Clim.*, **19**, 2144–2161.

Gregory, J. and M. Webb, 2008: Tropospheric adjustment induces a cloud component in CO_2 forcing. *J. Clim.*, **21**, 58–71.

Gregory, J. M., et al., 2004: A new method for diagnosing radiative forcing and climate sensitivity. *Geophys. Res. Lett.*, **31**, L03 205, doi:10.1029/2003GL018 747.

Hansen, J. E., A. Lacis, D. Rind, G. Russell, P. Stone, I. Fung, R. Ruedy, and J. Lerner, 1984: Climate sensitivity: Analysis of feedback mechanisms. In *Climate Processes and Climate Sensitivity*, AGU Geophysical Monograph 29, Maurice Ewing Vol. 5. J. E. Hansen and T. Takahashi, Eds. American Geophysical Union, 130-163 pp.

Harnik, N., R. Seager, N. Naik, M. Cane, and M. Ting, 2010: The role of linear wave refraction in the transient eddy-mean flow response to tropical Pacific SST anomalies. *Quart. J. Roy. Meteor. Soc.*, 136: 2132C2146. doi: 10.1002/qj.688.

Haynes, P. H., M. E. McIntyre, T. G. Shepherd, C. J. Marks, and K. P. Shine, 1991: On the downward control of extratropical diabatic circulations by eddy-induced mean zonal forces. *J. Atmos. Sci.*, **48**, 651–678.

Held, I. M., 1993: Large-scale dynamics and global warming. *Bull. Amer. Meteor. Soc.*, **74**, 228–241.

Held, I. M. and B. J. Soden, 2006: Robust Response of the Hydrological Cycle to Global Warming. *J. Clim.*, **19**, 5686–5699.

Hu, Y. and Q. Fu, 2007: Observed poleward expansion of the Hadley circulation since 1979. *Atmos. Chem. Phys.*, **7**, 5229–5236.

Hurrell, J. W., J. J. Hack, A. S. Phillips, J. Caron, and J. Yin, 2006: The dynamical simulation of the Community Atmosphere Model version 3 (CAM3). *J. Clim.*, **19**, 2162C2183.

Kushner, P. J., I. M. Held, and T. L. Delworth, 2001: Southern Hemisphere atmospheric circulation response to global warming. *J. Clim.*, **14**, 2238–2249.

Lorenz, D. J. and E. T. DeWeaver, 2007: Tropopause height and zonal wind response to global warming in the IPCC scenario integrations. *J. Geophys. Res.*, **112**, D10 119, doi:10.1029/2006JD008 087.

Lu, J., G. Chen, and D. M. W. Frierson, 2008: Response of the zonal mean atmospheric circulation to El Nino versus global warming. *J. Clim.*, **21**, 5835–5851.

Lu, J., G. A. Vecchi, and T. Reichler, 2007: Expansion of the Hadley cell under global warming. *Geophys. Res. Lett.*, **34**, L06 805, doi:10.1029/2006GL028 443.

Manabe, S., K. Bryan, and M. J. Spelman, 1990: Transient response to a global ocean-atmosphere model to a doubling of atmosphere carbon dioxide. *J. Phys. Oceanogr.*, **20**, 722–749.

McCaa, J. R., M. Rothstein, B. E. Eaton, J. M. Rosinski, E. Kluzek, and M. Vertenstein, 2004: User's guide to the NCAR Community Atmosphere Model (CAM3.0). Tech. rep., Climate And Global Dynamics Division, National Center For Atmospheric Research, Boulder, Colorado, USA.

McLandress, C., T. G. Shepherd, J. F. Scinocca, D. A. Plummer, M. Sigmon, A. I. Jonsson, and M. C. Reader, 2011: Separating the dynamical effects of climate change and ozone depletion. Part II: Southern Hemisphere troposphere. *J. Clim.*, **24**, 1850–1868.

Meehl, G., C. Covey, T. Delworth, M. Latif, B. McAvaney, J. F. B. Mitchell, R. J. Stouffer, and K. E. Taylor, 2007a: WCRP CMIP3 multimodel dataset: A new era in climate change research. *Bull. Amer. Meteor. Soc.*, **88**, 1383–1394.

Meehl, G. A. and W. M. Washington, 1996: El Nino-like climate change in a model with increased atmospheric CO_2 concentrations. *Nature*, **382**, 56–60.

Meehl, G. A., et al., 2007b: Global climate projections. *Climate Change 2007: The Physical Science Basis. Contribution of Working Group I to the Fourth Assessment Report of the Intergovernmental Panel on Climate Change*, S. Solomon, D. Qin, M. Manning, Z. Chen, M. Marquis, K. B. Averyt, M. Tignor, and H. L. Miller, Eds., Cambridge University Press, Chap. 10, 747–846.

O'Gorman, P. A., 2010: Understanding the varied response of the extratropical storm tracks to climate change. *Proc. Natl. Acad. Sci. U. S. A.*, **107**, 19 176–19 180.

Polvani, L., D. Waugh, G. Correa, and S.-W. Son, 2011: Stratospheric ozone depletion: the main driver of 20th century atmospheric circulation changes in the Southern Hemisphere. *J. Clim.*, **24**, 795–812, doi: 10.1175/2010JCLI3772.1.

Rasch, P. J., et al., 2006: A characterization of tropical transient activity in the CAM3 atmospheric hydrologic cycle. *J. Clim.*, **19**, 2222–2242.

Reichler, T., M. Dameris, and R. Sausen, 2003: Determining the tropopause height from gridded data. *Geophys. Res. Lett.*, **30**, 2042, doi:10.1029/2003GL018 240.

Sassi, F., R. R. Garcia, D. Marsh, and K. W. Hoppel, 2010: The role of the Middle Atmosphere in simulations of the troposphere during Northern Hemisphere winter: differences between high- and low-top models. *J. Atmos. Sci.*, **67**, 3048–3064.

Seager, R., N. Harnik, Y. Kushnir, W. Robinson, and J. Miller(Nakamura), 2003: Mechanisms of hemispherically symmetric climate variability. *J. Clim.*, **16**, 2960–2978.

Seager, R. and N. Naik, 2011: A mechanisms-based approach for detecting recent anthropogenic hydroclimate change. *J. Clim.*, submitted (revised in May 2011).

Seager, R., N. Naik, W. Baethgen, A. Robertson, Y. Kushnir, J. Nakamura, and S. Jurburg, 2010a: Tropical oceanic causes of interannual to multidecadal precipitation variability in southeast South America over the past century. *J. Clim.*, **23**, 5517–5539.

Seager, R., N. Naik, M. Ting, M. A. Cane, N. Harnik, and Y. Kushnir, 2010b: Adjustment of the atmospheric circulation to tropical Pacific SST anomalies: Variability of transient eddy propagation in the Pacific-North America sector. *Quart. J. Roy. Meteor. Soc.*, **136**, 277–296. DOI: 10.1002/qj.588.

Seager, R., N. Naik, and G. A. Vecchi, 2010c: Thermodynamic and dynamic mechanisms for large-scale changes in the hydrological cycle in response to global warming. *J. Clim.*, **23(17)**, 4651–4668.

Seager, R., et al., 2009: Mexican drought: an observational modeling and tree ring study of variability and climate change. *Atmosfera*, **22(1)**, 1–31.

Shaw, T. A. and J. Perlwitz, 2010: The impact of stratospheric model configuration on planetary scale waves in northern hemisphere winter. *J. Clim.*, **23**, 3369–3389.

Shindell, D. T., R. L. Miller, G. A. Schmidt, and L. Pandolfo, 1999: Simulation of recent northern winter climate trends by greenhouse-gas forcing. *Nature*, **399**, 452–455.

Shindell, D. T., G. A. Schmidt, R. L. Miller, and D. Rind, 2001: Northern Hemisphere winter climate response to greenhouse gas, ozone, solar, and volcanic forcing. *J. Geophys. Res.*, **106**, 7193–7210, doi:10.1029/2000JD900 547.

Sigmond, M., J. F. Scinocca, and P. J. Kushner, 2008: Impact of the stratosphere on tropospheric climate change. *Geophys. Res. Lett.*, **35**, L12 706, doi:10.1029/2008GL033 573.

Sigmond, M., P. C. Siegmund, E. Manzini, and H. Kelder, 2004: A simulation of the separate climate effects of middle-atmospheric and tropospheric CO_2 doubling. *J. Clim.*, **17**, 2352–2367.

Vecchi, G. A. and B. J. Soden, 2007: Global warming and the weakening of the tropical circulation. *J. Clim.*, **20(17)**, 4316–4340.

Williams, G. P., 2006: Circulation sensitivity to tropopause height. *J. Atmos. Sci.*, **63**, 1954–1961.

Wu, Y., M. Ting, R. Seager, H.-P. Huang, and M. A. Cane, 2010: Changes in storm tracks and energy transports in a warmer climate simulated by the GFDL CM2.1 model. *Clim. Dyn.*, DOI 10.1007/s00 382–010–0776–4.

Yin, J. H., 2005: A consistent poleward shift of the storm tracks in simulations of 21st century climate. *Geophys. Res. Lett.*, **32**, L18 701, doi:10.1029/2005GL023 684.

List of Tables

TABLE 1. 14 IPCC AR4 coupled models and their resolution for the atmospheric component used in this study.

Model	Atmospheric Resolution
CCCma CGCM3.1 T47	T47L31
CCCma CGCM3.1 T63	T63L31
CNRM-CM3	T63L45
CSIRO Mk3.5	T63L18
GFDL CM2.0	$2.5^o \times 2^o$L24
GFDL CM2.1	$2.5^o \times 2^o$L24
GISS-AOM	$4^o \times 3^o$L12
GISS-ER	$5^o \times 4^o$L20
IAP FGOALS	T42L26
IPSL CM4A	$2.5^o \times 3.75^o$L19
MIUBECHOG	T30L19
MIROC3.2(medres)	T42L20
MPI ECHAM5	T63L31
MRI CGCM2.3	T42L30

List of Figures

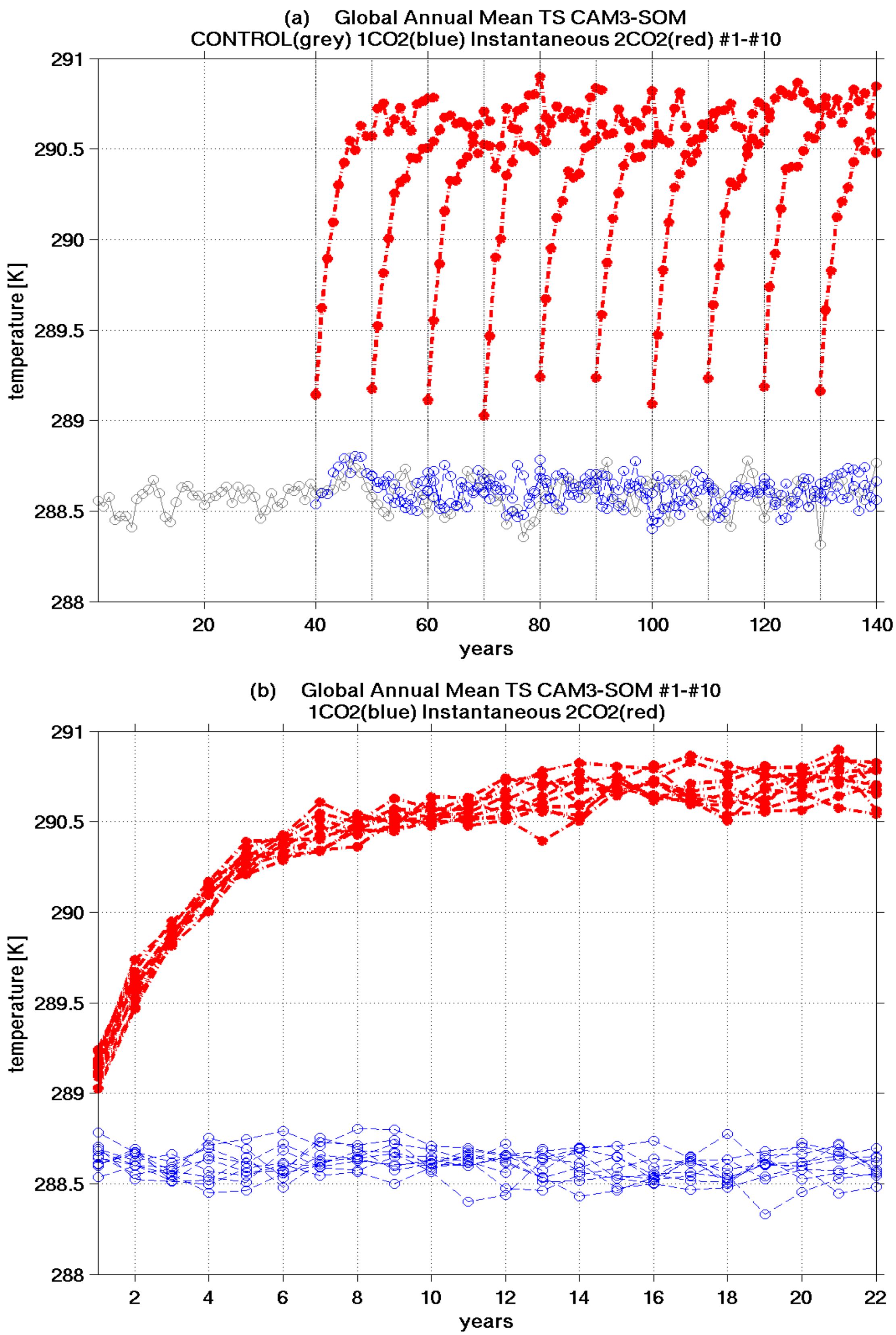

FIG. 1. The global annual mean surface temperature T_s for the control experiment for 140 years (grey lines), 10 of the 100 $1CO_2$ climatological runs (each for 22 years) (blue lines) and instantaneous $2CO_2$ runs (each for 22 years) (red lines) (a). Same for (b) except that they are shifted to the same starting year (year 1) and last for 22 years.

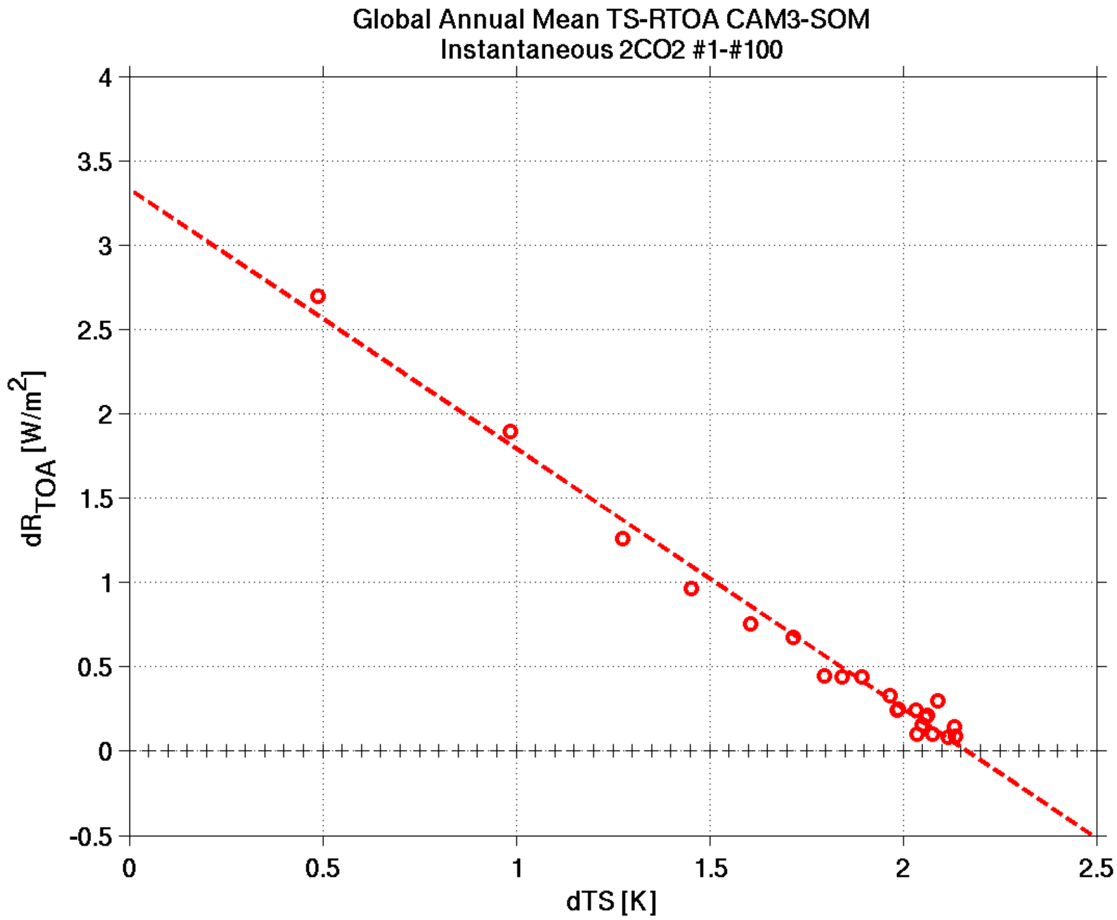

Fig. 2. Scatter plot for the ensemble mean change in global annual mean surface temperature T_s and the change in global annual mean net radiative flux at the top of the atmosphere (TOA) for the 22 years of integration. It provides an estimate for the doubling CO_2 forcing $F_{2\times} = 3.33$ W/m^2 and the climate sensitivity of about 2.2 K.

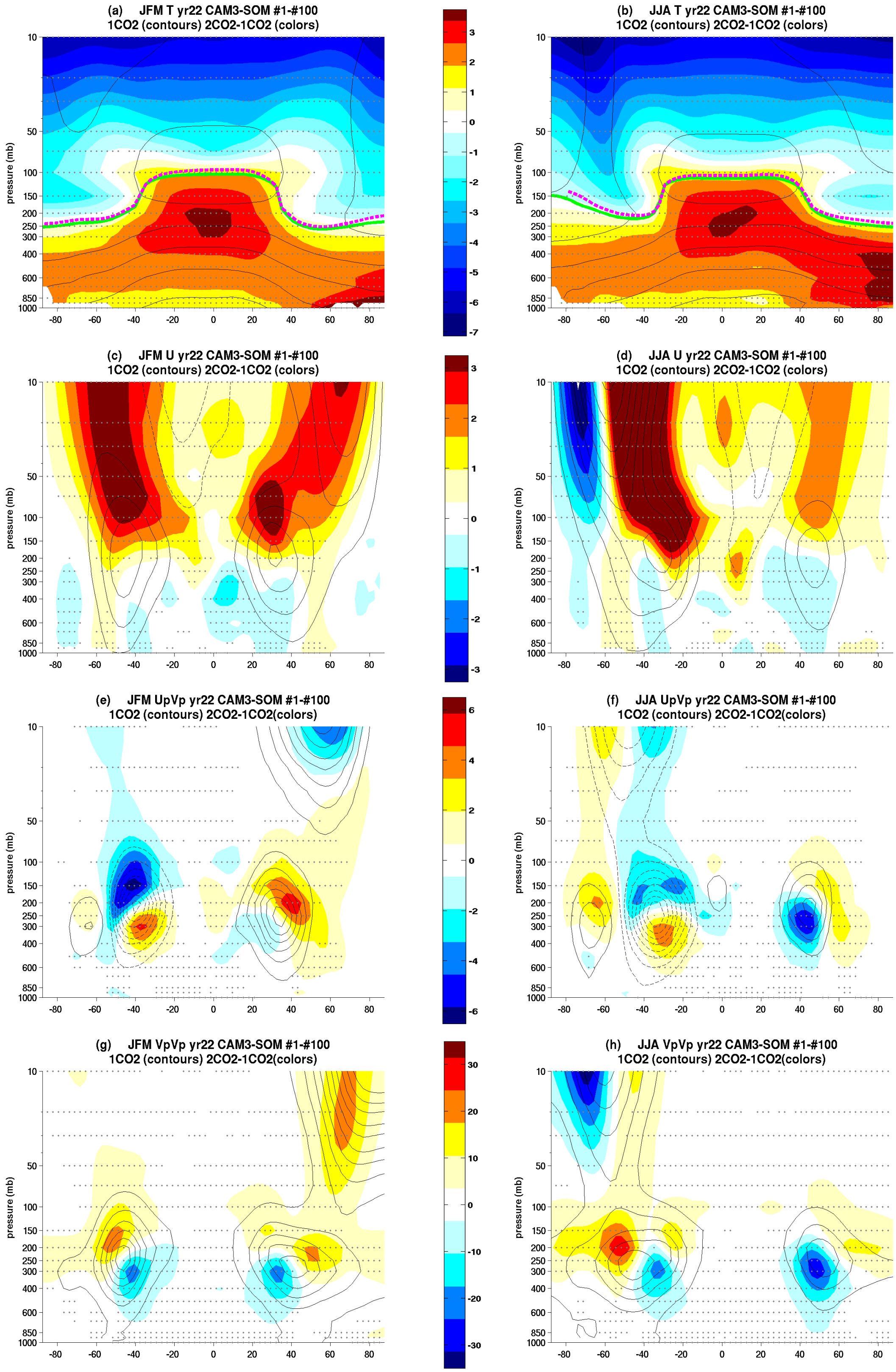

FIG. 3. The equilibrium response to a CO_2 doubling in (a)(b) $\langle \bar{T} \rangle$, (c)(d) $\langle \bar{u} \rangle$, (e)(f) $\langle \overline{u'v'} \rangle$ and (g)(h) $\langle \overline{v'v'} \rangle$ averaged over 100 members in January-February-March (JFM) (left) and June-July-August (JJA) (right) as a function of latitude and pressure level (mb). The tropopause level is plotted in green (dashed magenta) lines for the $1CO_2$ ($2CO_2$) runs. The colors show the difference between the $2CO_2$ and the $1CO_2$ runs and the contours show the climatology. The contour intervals are 20 K for (a)(b), 10 m/s for (c)(d), 10 m^2/s^2 for (e)(f) and 50 m^2/s^2 for (g)(h). The grey dots indicate the 95% significance level for the difference.

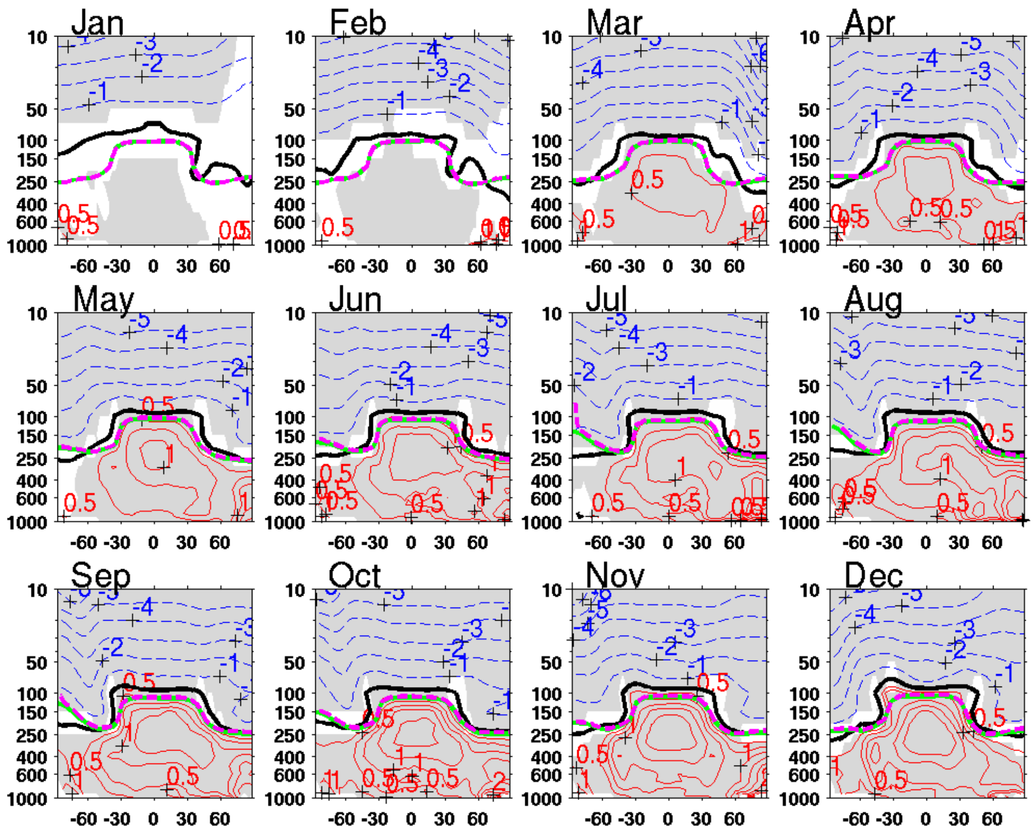

FIG. 4. The monthly transient response in year 1 after the instantaneous doubling of CO_2 on January 1st in zonal mean T, averaged over 100 ensemble members as a function of latitude (degree) and pressure level (mb). The color contours are the difference between the $2CO_2$ runs and the $1CO_2$ runs and the thick black contours are the zero value lines. The tropopause height is plotted in thick green (dashed magenta) lines for the $1CO_2$ ($2CO_2$) runs. The grey shadings show the 95% significance level. The red (dashed blue) contour intervals are 0.25 K for positive values and -1 K for negative values.

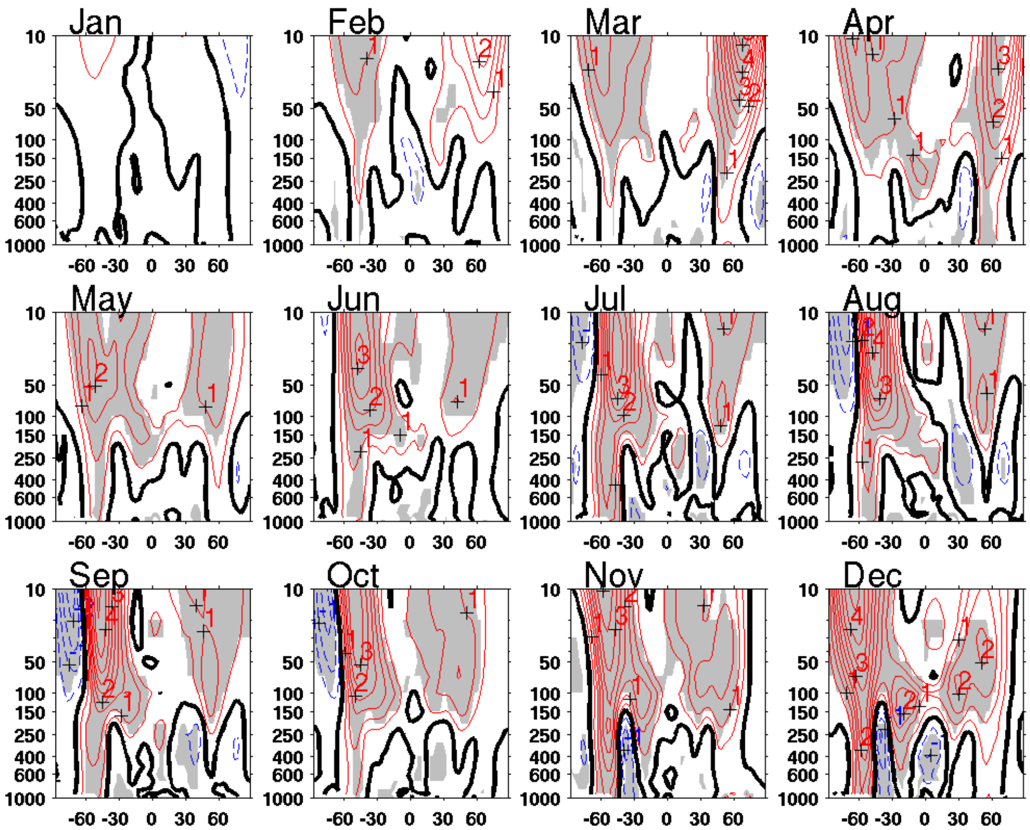

FIG. 5. Same as Figure 4 for but the monthly transient response in zonal mean zonal wind. The contour interval is 0.5 m/s.

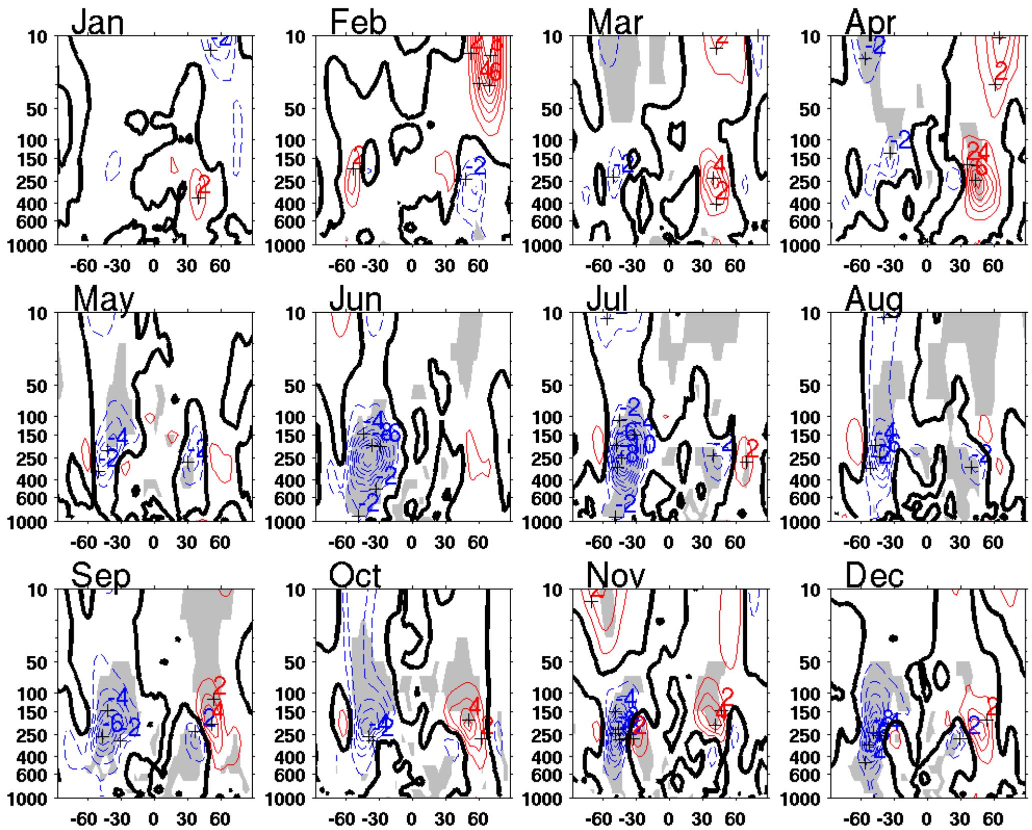

Fig. 6. Same as Figure 4 for but the monthly transient response in zonal mean transient eddy momentum flux ($\langle \overline{u'v'} \rangle$). The contour interval is 1 m^2/s^2.

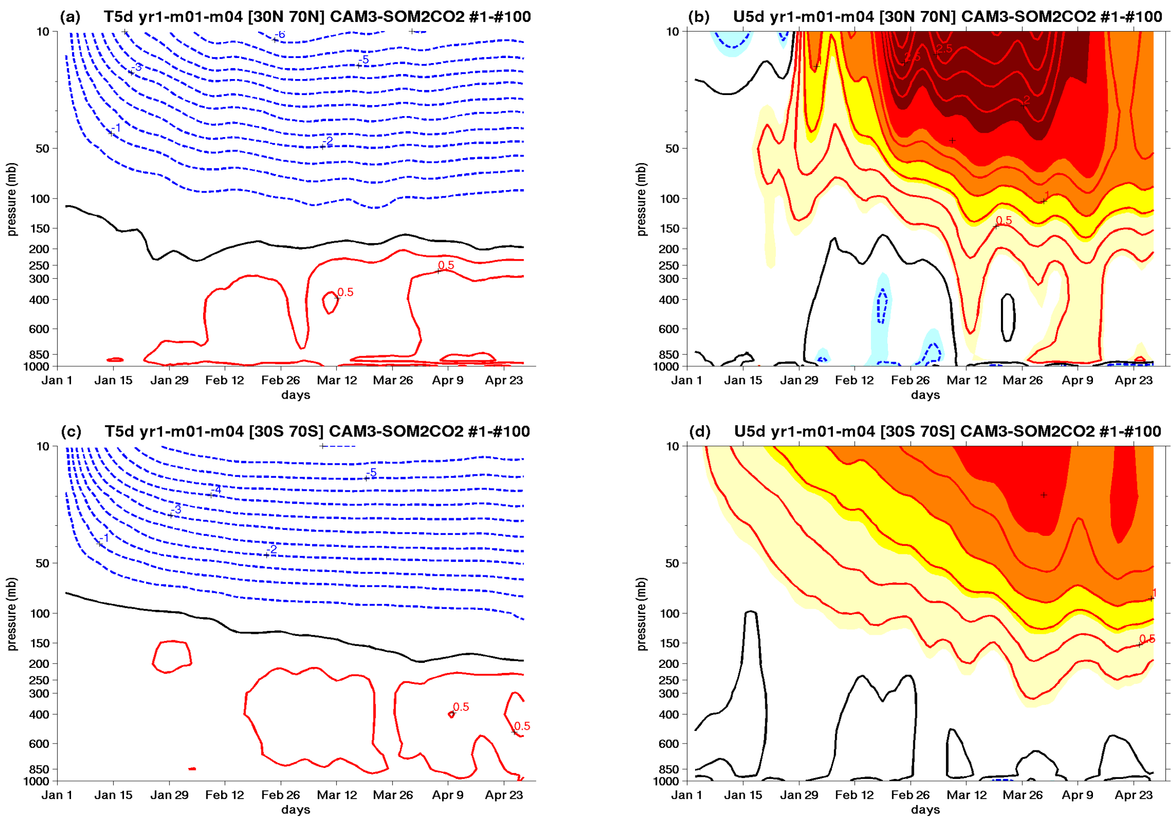

FIG. 7. The transient day-by-day response to CO_2 doubling in zonal mean temperature and zonal wind averaged between 30^{o}N and 70^{o}N (a)(b) and between 30^{o}S and 70^{o}S (c)(d). It is shown as a function of days from January 1st to April 30th and pressure levels (mb). A 5-day running average has been applied for plotting. The contour intervals are 0.25 K (0.5 K) for positive (negative) values in (a)(c) and 0.5 m/s for (b)(d).

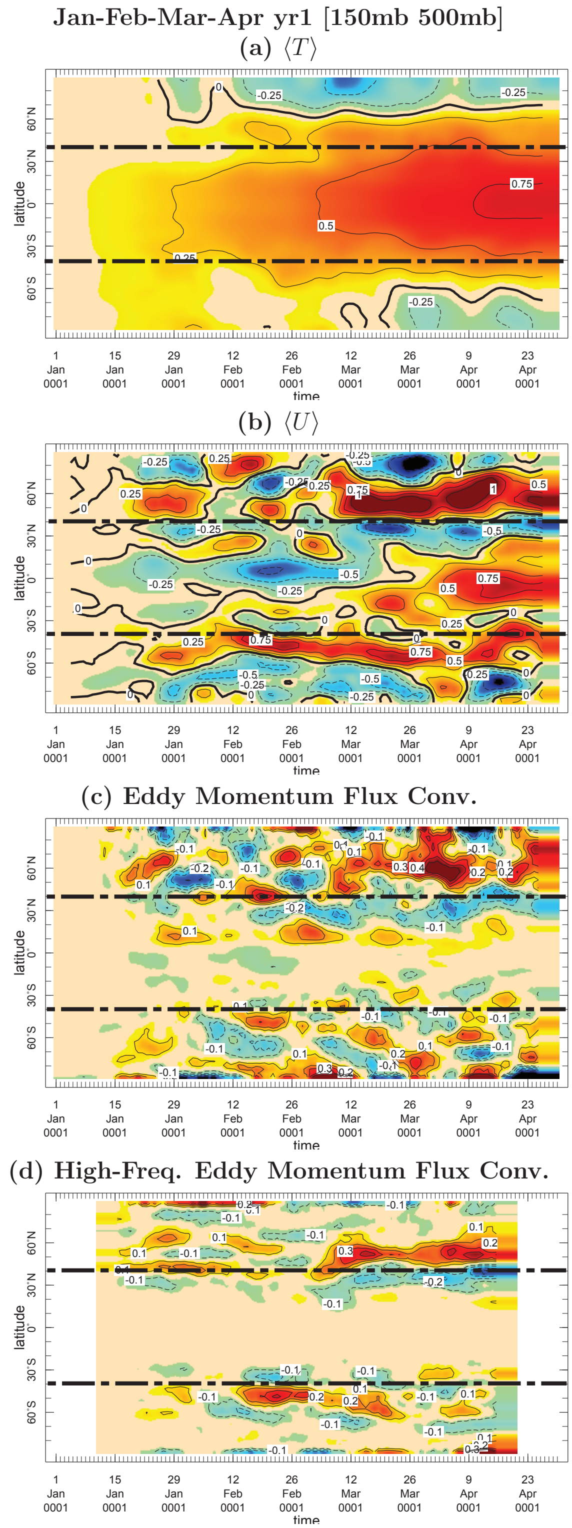

FIG. 8. The transient day-by-day response in January-February-March-April (JFMA) of year 1 in zonal mean (a) temperature, (b) zonal wind, (c) eddy momentum flux convergence, and (d) high-pass filtered eddy momentum flux convergence (defined in text) as a function of days and latitudes. They are averaged in the middle and upper troposphere from 150mb to 500mb, and a 10-day running average is applied. Latitude of 40^oN(S) is highlighted in dashed lines. The contour intervals are (a) 0.25 K, (b) 0.25 m/s and (c)(d) 0.25 m/s/day.

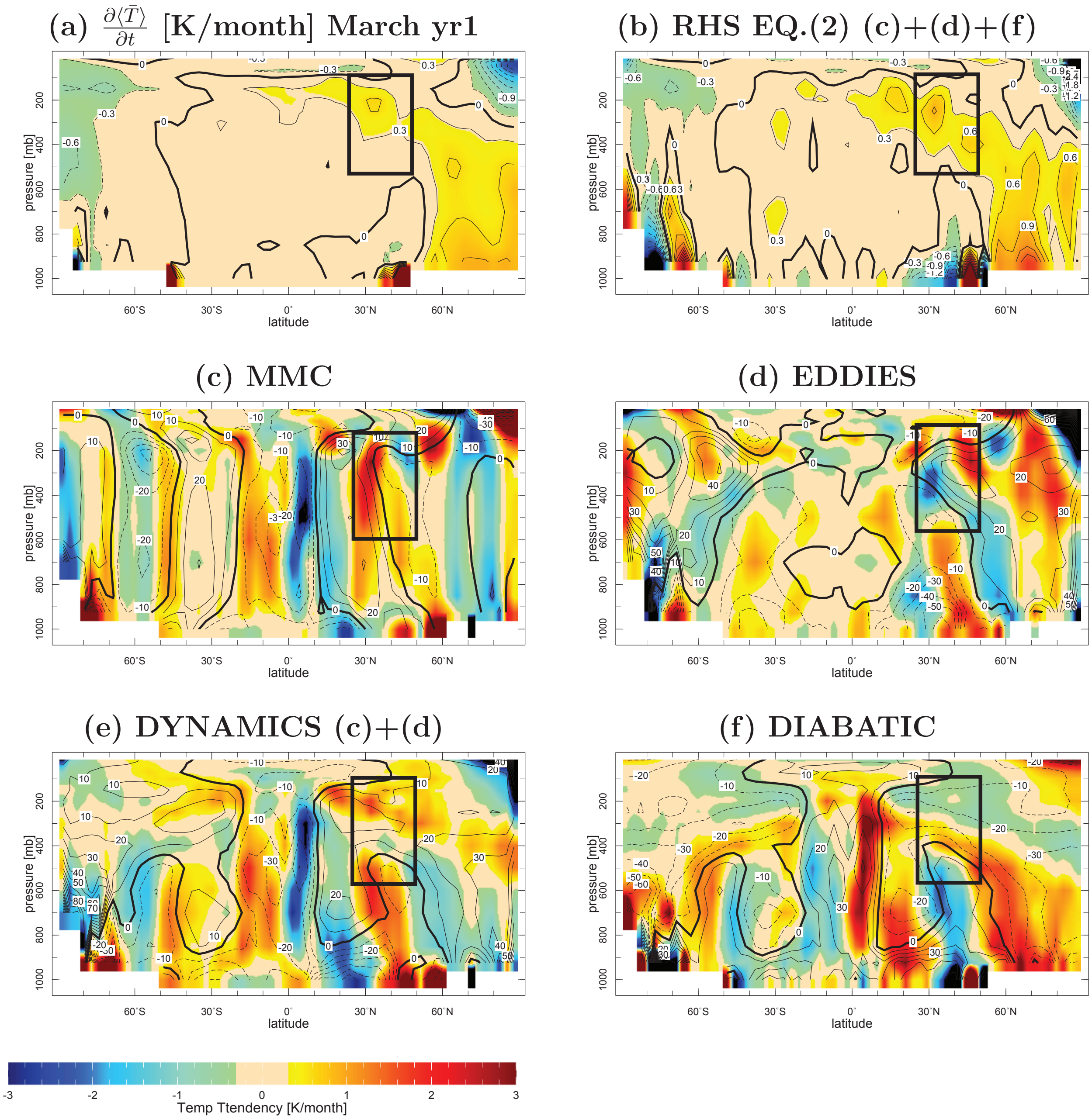

FIG. 9. (a) The actual zonal mean temperature tendency (T-tendency) [K/month] ($\frac{\partial\langle\bar{T}\rangle}{\partial t}$), (b) the T-tendency in sum of (c)(d)(f), T-tendencies due to (c) mean meridional circulation (MMC), (d) total eddies (stationary and transient eddies) and (f) total diabatic heating. (e) T-tendency due to the dynamics which is sum of (c) and (d). The plots are all for March of year 1. The contours and colors in (a) and (b) both show the instantaneous $2CO_2$ response with contour interval of 0.3 K/month. The colors in (c)(d)(e)(f) show the instantaneous $2CO_2$ response with the black contours the climatological response from the $1CO_2$ runs.

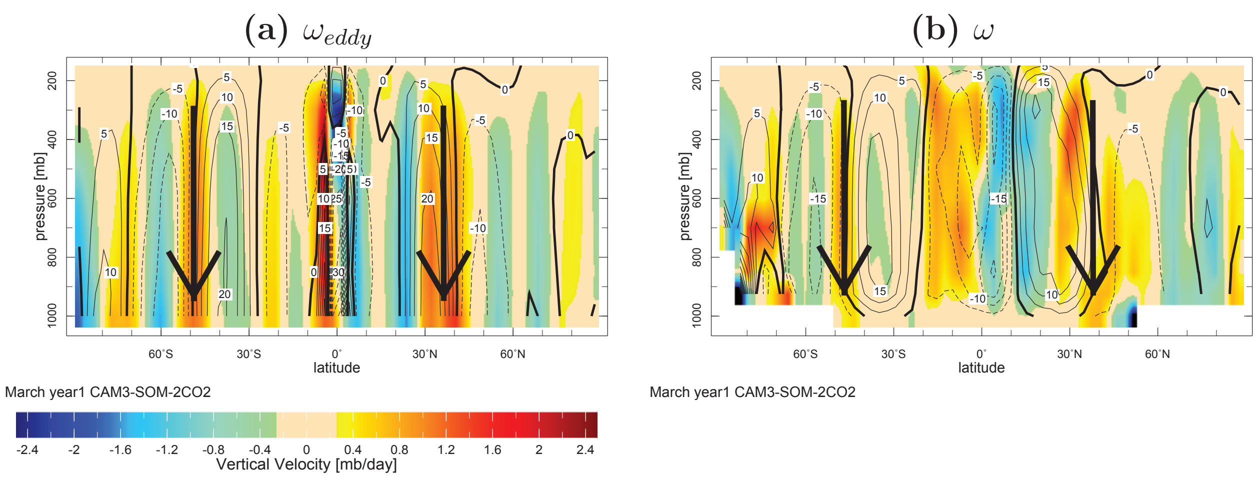

FIG. 10. (a) The transient eddy driven vertical motion ω_{eddy} [mb/day] and (b) the actual vertical motion ω [mb/day] from model output in March of year 1. The contours show the response from the climatological $1CO_2$ runs and the colors show the difference between the $2CO_2$ runs and the $1CO_2$ runs. The contour interval is 5 mb/day. The positive (negative) values denote downward (upward) motion.

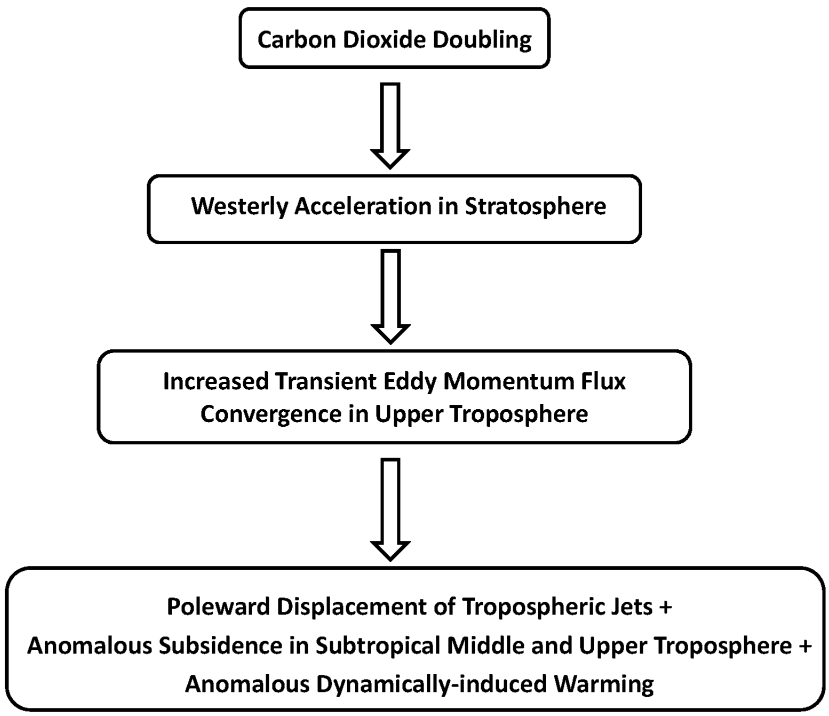

FIG. 11. Summary of the proposed mechanisms causing the tropospheric extratropical circulation response to increased CO_2 concentration.

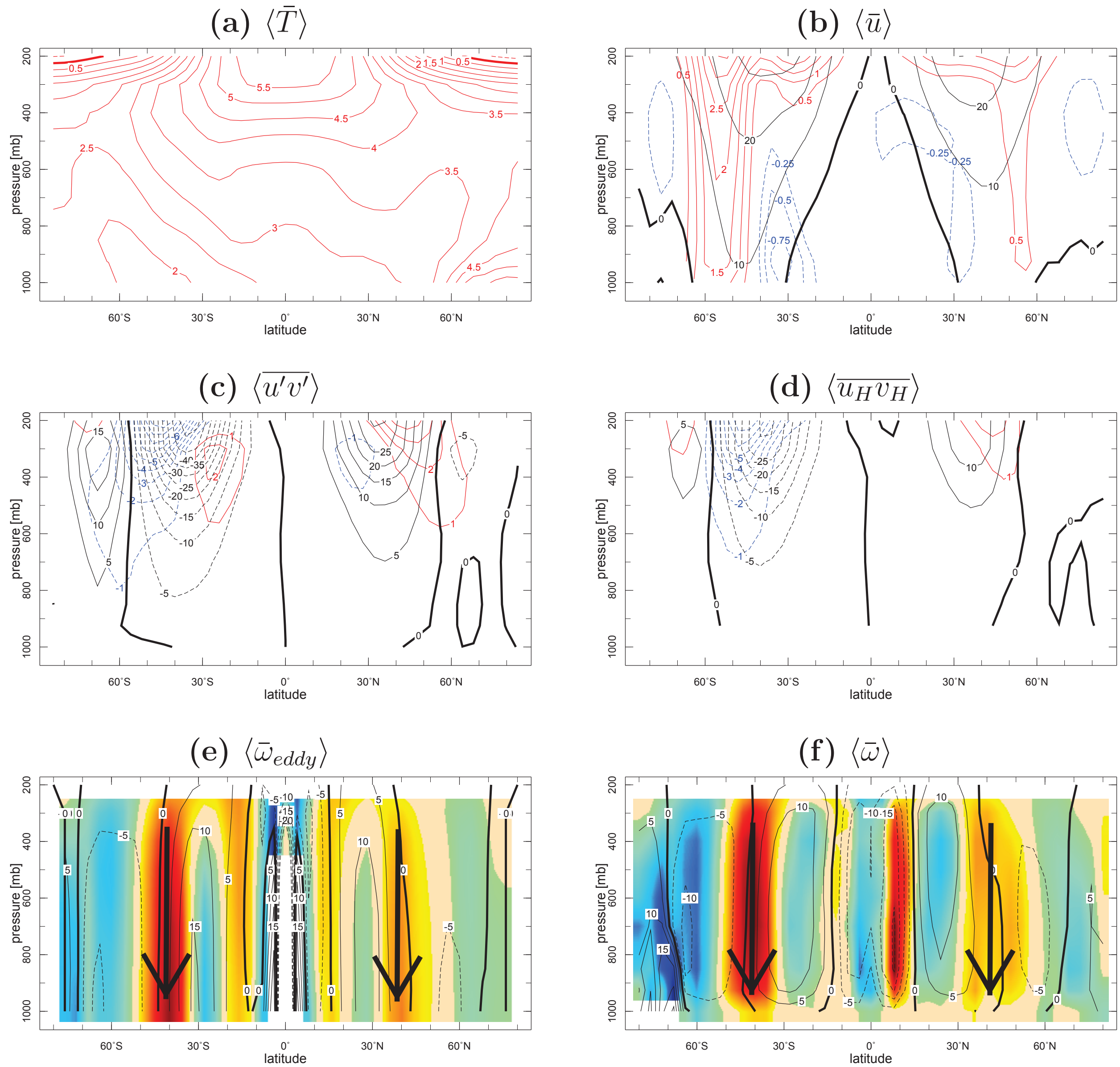

FIG. 12. The late 21st century trend in annual and zonal mean (a) T [K], (b) u [m/s], (c) transient eddy momentum flux $\langle \overline{u'v'} \rangle$ [m^2/s^2], (d) high-pass filtered transient eddy momentum flux $\langle \overline{u_H v_H} \rangle$ [m^2/s^2], (e) eddy-driven vertical motion $\langle \bar{\omega}_{eddy} \rangle$ [mb/day] and (f) model output $\langle \bar{\omega} \rangle$ [mb/day] averaged in 14 CMIP3/IPCC AR4 coupled models. The black contours show the average of 1961-2000 and the color contours (shadings) show the difference between 2081-2100 (SRES A1B) and 1961-2000. The color scale in (e)(f) is the same as in Figure 10. It is noted that the pressure level is up to 200mb due to availability of daily variables.